

## Wave-Vector-Dependent Exciton Exchange Interaction

G. Dasbach,<sup>1</sup> D. Fröhlich,<sup>1</sup> H. Stolz,<sup>2</sup> R. Klieber,<sup>1</sup> D. Suter,<sup>1</sup> and M. Bayer<sup>1</sup>

<sup>1</sup>*Institut für Physik, Universität Dortmund, D-44221 Dortmund, Germany*

<sup>2</sup>*Fachbereich Physik, Universität Rostock, D-18051 Rostock, Germany*

(Received 8 April 2003; published 4 September 2003)

The exchange interaction for the yellow 1S orthoexciton in Cu<sub>2</sub>O is derived up to the order  $K^2$ . The resulting exchange splittings are verified experimentally using high resolution spectroscopy. In agreement with theory the fine structure shows a characteristic dependence on the direction of the wave vector.

DOI: 10.1103/PhysRevLett.91.107401

PACS numbers: 78.20.-e, 71.35.Cc, 78.40.Fy

Exchange interaction couples the spins of electron and hole, which gives rise to an exciton fine structure. This fine structure has been studied intensely. Investigations beginning with bulk semiconductors [1,2] have been extended to quantum wells [3] and recently further to quantum dots [4]. Exchange interaction splits excitonic levels of different total angular momenta. Because of the complexity of the semiconductor band structure difficulties in calculating the electron-hole exchange microscopically arise. Attempts to describe it on a quantitative level can hardly be found [5]. In higher dimensional structures exchange interaction is normally treated as a wave vector independent spin-spin interaction, which is in agreement with the experiments reported so far. These studies, however, were performed with modest spectral resolution of typically  $\approx 20 \mu\text{eV}$ . Spectroscopic studies of exchange are often difficult as the energy splittings involved are rather small. In addition, difficulties arise from a limited crystal quality. Cu<sub>2</sub>O is the prototype material for exciton physics [6], due to its high crystal quality and large binding energy of 150 meV. Hence, it seems ideally suited for the study of electron-hole exchange and its wave vector ( $\mathbf{K}$ ) dependence.

In this Letter, we present transmission studies of the 1S ground state of the yellow exciton series in Cu<sub>2</sub>O. Using a single frequency dye laser we achieve a spectral resolution of  $\approx 5 \text{ neV}$ . At this extreme resolution the linewidth of the transition is found to be much smaller than measured previously ( $< 1 \mu\text{eV}$  FWHM at  $T = 1.4 \text{ K}$ ). More strikingly, the orthoexciton, so far treated as threefold degenerate in unstrained samples, shows a characteristic fine structure, where the splitting critically depends on the direction of the wave vector. We demonstrate that the fine structure arises from  $\mathbf{K}$ -dependent exchange interaction, to our knowledge never observed before in any excitonic system.

The yellow 1S excitons are formed by a hole in the valence band ( $\Gamma_7^+$ ) and an electron in the conduction band ( $\Gamma_6^+$ ). Consequently, the exciton is decomposed into a  $\Gamma_2^+$  and a  $\Gamma_5^+$  representation [7]. The so-called paraexciton ( $\Gamma_2^+$ ) is optically forbidden. The threefold orthoexciton ( $\Gamma_5^+$ ) is quadrupole allowed [8], leading to a small oscil-

lator strength and little radiative broadening as compared to dipole-allowed transitions [9].

Despite the quadrupole character, the exciton-photon interaction leads to coupled modes, the polaritons. Their dispersion depends on the exciton oscillator strength and  $\mathbf{K}$ . The amplitudes ( $QA_1$  to  $QA_3$ ) of the orthoexciton quadrupole transitions are given by the symmetric vector product of  $\mathbf{K}$  and the polarization vector  $\mathbf{e}$  [8]:

$$\begin{pmatrix} QA_1 \\ QA_2 \\ QA_3 \end{pmatrix} = \begin{pmatrix} e_y K_z + e_z K_y \\ e_z K_x + e_x K_z \\ e_x K_y + e_y K_x \end{pmatrix}. \quad (1)$$

We will now derive the electron-hole exchange up to the order  $K^2$ . It is given by the Coulomb interaction of the charge distributions  $\rho$  and  $\rho'$  [1],

$$J_{ex} = \delta_{\mathbf{K},\mathbf{K}'} \sum_{\mathbf{R}} e^{i\mathbf{K}\cdot\mathbf{R}} \iint \frac{\rho^*(\mathbf{r}_1)\rho'(\mathbf{r}_2)d\mathbf{r}_1d\mathbf{r}_2}{|\mathbf{r}_1 + \mathbf{r}_2 - \mathbf{R}|}, \quad (2)$$

with the lattice vectors  $\mathbf{R}$ , where the orthoexciton exchange is determined by the interaction of the spin-singlet exciton charge distributions. Introducing the Fourier transform  $M(\mathbf{K}) = \int d\mathbf{r}\rho(\mathbf{r})\exp(-i\mathbf{K}\cdot\mathbf{r})$ , the exchange integral is transformed into a sum over the reciprocal lattice vectors  $\mathbf{K}_n$  [1],

$$J_{ex} = \delta_{\mathbf{K},\mathbf{K}'} \frac{4\pi}{\Omega} \sum_n \frac{M^*(\mathbf{K} + \mathbf{K}_n)M'(\mathbf{K} + \mathbf{K}_n)}{(\mathbf{K} + \mathbf{K}_n)^2}. \quad (3)$$

First, we concentrate on the long-range (LR) exchange ( $\mathbf{K}_n = 0$ ). Expanding  $\exp(-i\mathbf{K}\cdot\mathbf{r})$  into spherical harmonics  $Y_{l,m}$  and decomposing  $\rho$  into multipoles [10], the LR quadrupole-quadrupole ( $l = 2$ ) exchange energy is given by

$$J_{ex}^Q = \delta_{\mathbf{K},\mathbf{K}'} \frac{16\pi^2}{45\Omega} K^2 \sum_{m_1, m_2 = -2}^2 q_{m_1}^* q_{m_2} Y_{2, m_1}^*(\theta, \phi) Y_{2, m_2}(\theta, \phi), \quad (4)$$

where  $\theta$  and  $\phi$  are the spherical angles of  $\mathbf{K}$  with respect to the cubic axes and  $q_m = \sqrt{4\pi/5} \int d\mathbf{r} r^2 Y_{2,m}^* \rho(\mathbf{r})$  denote the quadrupole moments [10]. Then the matrix

representation of the exchange energy in the Cartesian orthoexciton basis  $\Gamma_{5yz}^+$ ,  $\Gamma_{5zx}^+$ ,  $\Gamma_{5xy}^+$  is given by

$$J_{ex}^O = \Delta_Q \cdot \frac{1}{K^2} \begin{pmatrix} K_z^2 K_y^2 & K_z^2 K_x K_y & K_z K_x K_y^2 \\ K_z^2 K_x K_y & K_z^2 K_x^2 & K_x^2 K_y K_z \\ K_z K_x K_y^2 & K_x^2 K_y K_z & K_x^2 K_y^2 \end{pmatrix}, \quad (5)$$

where  $\Delta_Q$  is the LR quadrupole-quadrupole exchange parameter. In contrast to dipole-allowed excitons, the quadrupole LR exchange scales as  $K^2$  and is therefore analytic at  $\mathbf{K} = 0$ . The paraexciton has zero spin-singlet charge density and hence is not affected by this interaction [11].

The  $\mathbf{K}_n \neq 0$  terms of Eq. (3) give the short-range (SR) exchange, which we expand into orders of  $\mathbf{K}$  and treat each order by the method of invariants [1,12]. The well known  $\mathbf{K}$ -independent SR contribution splits the paraexciton from the orthoexcitons by  $\Delta_0 = 12$  meV [13]; however, it leaves the orthoexcitons degenerate. The next higher order term would scale linearly with  $\mathbf{K}$ , but vanishes due to the inversion symmetry of the lattice (point group  $O_h$ ). The SR exchange of order  $K^2$  gives nonvanishing contributions: The electron and hole spins transform as  $\Gamma_4^+$ , while  $\mathbf{K}$  is a polar vector ( $\Gamma_4^-$ ). Consequently, the SR exchange is given by representations of  $\Gamma_1^+$ ,  $\Gamma_3^+$ ,  $\Gamma_4^+$ , and  $\Gamma_5^+$  [7]. The corresponding matrix representations  $J_1$ ,  $J_3$ ,  $J_4$ , and  $J_5$  are given below.

$J_1 = \Delta_1 K^2 \cdot \mathbf{1}$  causes a rigid shift of all orthoexciton states by an energy  $\Delta_1$ . It leads to an isotropic correction of the spatial dispersion and hence of the effective mass.  $J_3$  is given by

$$J_3 = \Delta_3 \cdot \begin{pmatrix} 3K_x^2 - K^2 & 0 & 0 \\ 0 & 3K_y^2 - K^2 & 0 \\ 0 & 0 & 3K_z^2 - K^2 \end{pmatrix}. \quad (6)$$

It has diagonal form, where the states have a distinctive  $\mathbf{K}$  dependence. Though  $J_3$  gives rise to an orthoexciton fine structure, no mixing of the states occurs.  $J_4$  vanishes as  $\mathbf{K}$  transforms as  $\Gamma_4^-$ . Finally,  $J_5$  is given by

$$J_5 = \Delta_5 \cdot \begin{pmatrix} 0 & K_x K_y & K_x K_z \\ K_x K_y & 0 & K_y K_z \\ K_x K_z & K_y K_z & 0 \end{pmatrix}. \quad (7)$$

$J_5$  has only off-diagonal terms and hence causes a  $\mathbf{K}$ -dependent mixing of the states. To summarize, we have derived three terms of order  $K^2$  that can give rise to an orthoexciton fine structure: the LR quadrupole interaction  $J_Q^{ex}$ , and the SR contributions  $J_3$ ,  $J_5$ , where the absolute splittings are determined by the exchange parameters  $\Delta_Q$ ,  $\Delta_3$ , and  $\Delta_5$ .

The  $\mathbf{K}$  dependence of the exchange can be investigated experimentally by an absorption experiment, where the laser beam propagating along  $\mathbf{K}$  directly probes the corresponding fine structure. The  $\mathbf{K}$  dependence of the exchange has not been resolved in experiments with limited

spectral resolution ( $\geq 20$   $\mu\text{eV}$ ). Thus the exchange splittings are expected not to be larger than a few  $\mu\text{eV}$ . To obtain such high resolution, we made use of a dye ring laser with a linewidth of  $\approx 5$  neV. The transmission was recorded while the laser energy was scanned across the orthoexciton resonances centered around 2.0327 eV. The absolute laser energy was adjusted within an accuracy of  $\approx 10$   $\mu\text{eV}$  by means of a wave meter. The measurements were performed on high-quality natural  $\text{Cu}_2\text{O}$  crystals, which were oriented by x-ray diffraction. After cutting and polishing most crystals had a cubic shape with extensions of  $\approx 4$  mm. The samples were excited by linearly polarized light  $\mathbf{e}(\psi)$ , where the polarization angle  $\psi$  could be adjusted ( $\psi = 0$  corresponds to horizontal  $\mathbf{e}$ ). Polarizers placed in front of the sample and between sample and detector ensured precise control of the exciting as well as detected polarization components. Both polarizers were kept parallel. By adjusting  $\mathbf{e}(\psi)$ , the relative amplitudes of the orthoexciton states could be controlled [Eq. (1)]. Rotating the samples around the vertical axis by an angle  $\varphi'$  gave access to intermediate  $K$  directions. The dependence of the orthoexciton energies  $E_1$ ,  $E_2$ , and  $E_3$  on  $\varphi$  (angle of laser beam inside the sample) could thus be measured. Special care was taken to ensure a strain free mounting in the helium bath cryostat ( $T = 1.4$  K).

For high symmetry  $\mathbf{K}$ 's the matrices (5)–(7) can be diagonalized analytically. For  $\mathbf{K} = (\bar{1}10)$  exchange interaction should lift the degeneracy of the orthoexcitons and three separate lines are expected [Fig. 1(a)]. This is investigated by the experiments presented in Fig. 2. Calculating  $|QA_2|^2$  shows that for  $\psi = -36^\circ$  [ $\mathbf{e}(-36^\circ) = (00\bar{1})$ ] the transition  $E_2$  is maximally allowed [Fig. 2(a)]. One indeed finds a strong absorption [full line in Fig. 2(c)] [14]. For  $\psi = +54^\circ$  the  $E_2$  transition is forbidden, as confirmed by the experiment [triangles in Fig. 2(c)]. The transitions  $E_1$  and  $E_3$  are forbidden for all  $\psi$ . For  $\varphi \neq 0$  and  $\psi = +54^\circ$ , however,  $E_1$  and  $E_3$  should become weakly allowed, while  $E_2$  remains forbidden [Fig. 2(b)].

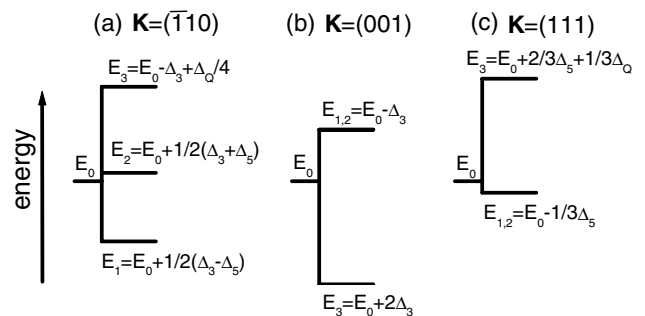


FIG. 1. Schematic energy level diagram of the exciton states.  $E_0$  gives the orthoexciton energy including the exchange shifts  $\Delta_0$  and  $\Delta_1$ . (a), (b), and (c) give the energy schemes for  $\mathbf{K} = (\bar{1}10)$ ,  $(001)$ , and  $(111)$ , respectively, ( $\Delta_Q = 5$   $\mu\text{eV}$ ,  $\Delta_3 = -1.3$   $\mu\text{eV}$ ,  $\Delta_5 = 2$   $\mu\text{eV}$ ).

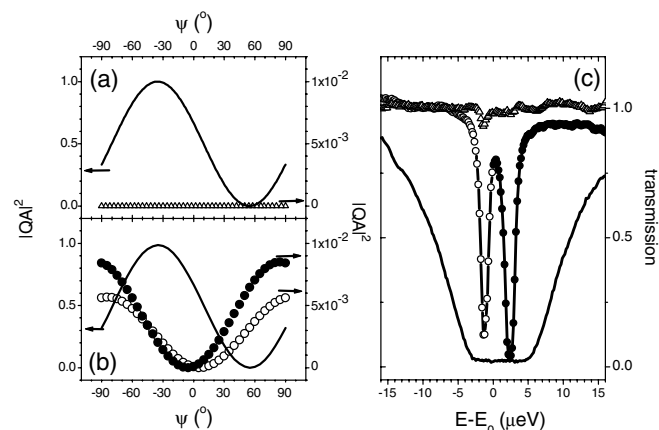


FIG. 2. (a) Calculated intensities  $|QA_1|^2$ ,  $|QA_2|^2$  (triangles), and  $|QA_3|^2$  (full line) as a function of  $\psi$  for  $\varphi = 0$ .  $\mathbf{K}(\varphi = 0)$  is along  $(\bar{1}10)$  and for  $\psi = 0$  the polarization vector  $\mathbf{e}(\psi)$  points along  $(11\bar{2})$ . (b) Calculated intensities  $|QA_2|^2$  (full line),  $|QA_1|^2$  (open dots), and  $|QA_3|^2$  (full dots) as a function of  $\psi$  for  $\varphi = 4^\circ$ . Note the different scales for  $|QA_1|^2$ ,  $|QA_3|^2$  (right scale), and  $|QA_2|^2$  (left scale). (c) Transmission spectra of a 4 mm thick crystal. The full line and the triangles show the transmission spectra for  $\psi = -36^\circ$  [ $\mathbf{e} = (00\bar{1})$ ] and  $\psi = 54^\circ$  [ $\mathbf{e} = (110)$ ], respectively, ( $\varphi = 0$ ). The spectrum for  $\psi = 54^\circ$  and  $\varphi = 4^\circ$  [rotation around  $(111)$  axis] is shown by open dots [ $E_1$  resonance in Fig. 1(a)] and full dots [ $E_3$  resonance in Fig. 1(a)].

The dots in Fig. 2(c) show the predicted  $E_1 - E_3$  doublet with a splitting of  $4.0 \mu\text{eV}$ . Both lines are extremely narrow with a width  $\lesssim 1 \mu\text{eV}$ .

Having demonstrated qualitative agreement between theory and experiment, we proceed with the quantitative analysis of  $\Delta_Q$ ,  $\Delta_3$ , and  $\Delta_5$ . For  $\mathbf{K} = (001)$ ,  $J_{\text{ex}}^Q$  and  $J_5$  vanish and the fine structure is determined only by  $J_3$ . It should give rise to two lines, as  $E_1$  and  $E_2$  remain degenerate [Fig. 1(b)], where  $E_{1,2}$  and  $E_3$  are split by  $3\Delta_3$ . Indeed, the expected fine structure is observed in the experiment [Fig. 3(a)]. The levels  $E_{1,2}$  and  $E_3$  are distinguished by analyzing  $|QA_{1,2}|^2$  and  $|QA_3|^2$  as a function of  $\mathbf{e}(\psi)$ , which allows one to determine the sign of  $\Delta_3 = -1.3 \mu\text{eV}$ . In the angular range investigated no significant line shifts are expected and the degeneracy of  $E_1$  and  $E_2$  is only slightly lifted, which is masked by their spectral width. For the sample orientation of Fig. 2  $E_1$ ,  $E_2$ , and  $E_3$  are shown as a function of  $\varphi$  in Fig. 3(b).  $E_2 - E_1$  gives directly  $\Delta_5 = 2 \mu\text{eV}$ . Finally,  $\Delta_Q = 5 \mu\text{eV}$  is determined from  $E_3$ . These parameters also give the correct relative line positions, when comparing the absolute energies obtained for  $\mathbf{K} = (001)$  to those for  $\mathbf{K} = (\bar{1}10)$  [15].

As a test of consistency, we present data for  $\mathbf{K} = (111)$  [Figs. 4(a)–4(d)]. According to Fig. 1(c) we expect for  $\varphi \rightarrow 0$  a degenerate level  $E_{1,2}$  plus a high energy state  $E_3$ . This is confirmed in Fig. 4(b). In agreement with theory  $E_{1,2}$  splits into a doublet for  $\varphi \neq 0$  [Figs. 4(a) and 4(c)]. As seen in Fig. 4(d) the  $E_1 - E_2$

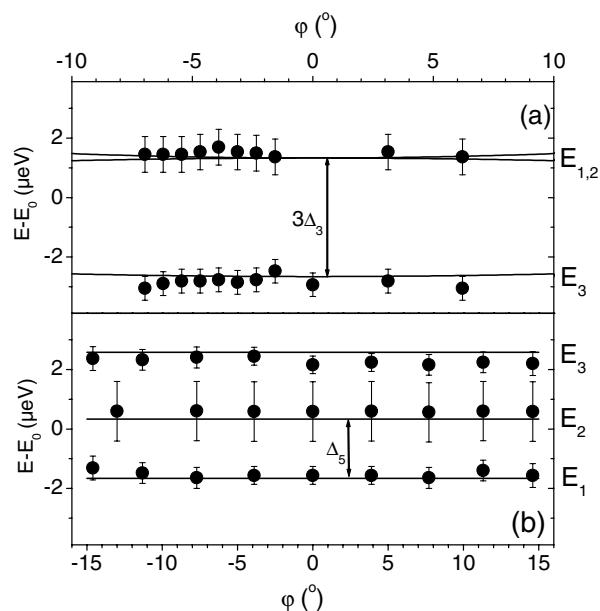


FIG. 3.  $E_1, E_2, E_3$  as a function of  $\varphi$  for 4 mm thick samples. Dots mark the experimental data. Full lines give the calculated values. (a) For  $\varphi = 0$ ,  $\mathbf{K}$  is along  $(001)$ .  $\varphi$  describes a rotation around the  $(1\bar{1}0)$  axis. (b) For  $\varphi = 0$ ,  $\mathbf{K}$  is along  $(\bar{1}10)$ .  $\varphi$  describes a rotation around the  $(111)$  axis.

splitting increases with  $|\varphi|$ , while  $E_3$  shows slight shifts. The fine structure is calculated (full lines) using the parameters obtained above. Obviously, the parameters allow a consistent description for these  $\mathbf{K}$  directions. To overcome the line broadening found for lines with large  $|QA|$  in Fig. 2(c) a thin sample had to be employed, which permits resolving the  $E_1 - E_2$  splitting [Figs. 4(a) and 4(c)].

The degeneracy of the orthoexciton could also be lifted by strain. However, several arguments rule out an interpretation of the observed fine structure as strain-induced: (i) Strain is expected to be inhomogeneous across the sample. In our experiments, however, the spectrum is unaltered when probing various sections of the crystals. In 4 mm thick samples a macroscopic volume of the specimen is probed and strain would give rise to an inhomogeneous broadening. However the lines remain extremely narrow and Lorentzian in shape. (ii) The impact of residual strain can be approached by symmetry considerations: The strain tensor has the same symmetry as the SR exchange. Therefore the effect of strain on the  $\Gamma_5^+$  states can be described by the three matrices  $\epsilon_1, \epsilon_3, \epsilon_5$ , where each  $k_m$  in  $J_1, J_3, J_5$  is replaced by a constant strain matrix element  $\epsilon_m$ . Strain-induced shifts can be discriminated from exchange as they depend only on the orientation of the crystalline axes, but not on  $\mathbf{K}$ . Therefore, when turning the crystal one would not expect any dependence of the energy levels on  $\varphi$  for strain induced effects, contrary to the experimental results [Fig. 4(d)].

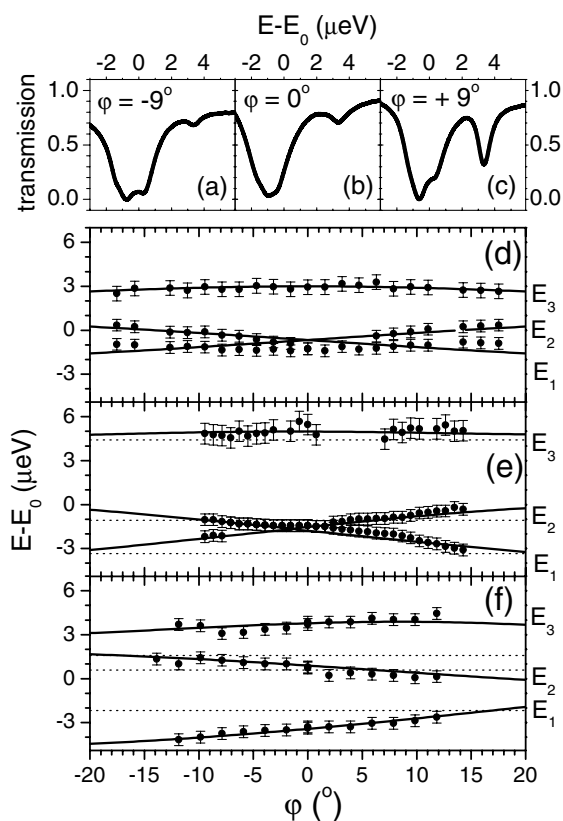


FIG. 4. Transmission spectra for  $\varphi = -9^\circ$  (a),  $0$  (b), and  $+9^\circ$  (c), where the sample (thickness  $85 \mu\text{m}$ ) was rotated around the  $(11\bar{2})$  axis and  $\mathbf{K}$  is along  $(111)$  at  $\varphi = 0$ . (d)  $E_1$ ,  $E_2$ , and  $E_3$  versus  $\varphi$ . (e)  $E_1$ ,  $E_2$ ,  $E_3$  as a function of  $\varphi$  for a slightly strained sample [thickness  $30 \mu\text{m}$ ,  $\mathbf{K} = (111)$  at  $\varphi = 0$ , axis of rotation  $(11\bar{2})$ ]. (f)  $E_1$ ,  $E_2$ ,  $E_3$  as a function of  $\varphi$  for a slightly strained sample [thickness  $95 \mu\text{m}$ ,  $\mathbf{K} = (\bar{1}10)$  at  $\varphi = 0$ , axis of rotation  $(\bar{1}10)$ ]. In each case, full dots give the data, while full lines mark the theory. In (e) and (f) theory includes strain induced effects and the calculated strain offsets are given by the dotted lines.

This can be demonstrated by repeating the experiment of Figs. 4(a)–4(d) on a slightly strained sample [Fig. 4(e)]. The data show a significantly larger  $E_{1,2} - E_3 \approx 7 \mu\text{eV}$  ( $\varphi = 0$ ) as compared to the unstrained sample. However, the same characteristic  $\mathbf{K}$  dependence is found. Calculations including exchange and strain give a very good description of the data. For the exchange contribution the parameters derived above have been used. Obviously, the  $\mathbf{K}$  dependence solely arises from exchange, while the increased splittings have to be attributed to stress induced offsets (dotted lines). As a crucial test of our analysis we have chosen a low symmetry  $K$  direction  $(11\bar{2})$ . As expected, we find three distinct lines

with a pronounced  $\varphi$  dependence. Again slight strain-induced offsets are found (dotted lines), while the  $\mathbf{K}$  dependencies of the orthoexciton energies are well described by our set of parameters.

In conclusion, we have derived and demonstrated  $K^2$ -dependent exchange interaction of excitons. For the yellow  $1S$  orthoexcitons in  $\text{Cu}_2\text{O}$  the exchange parameters  $\Delta_Q = 5 \pm 1.5 \mu\text{eV}$ ,  $\Delta_3 = -1.3 \pm 0.2 \mu\text{eV}$ , and  $\Delta_5 = 2 \pm 0.3 \mu\text{eV}$  are obtained, where the errors are estimated by evaluating several experiments performed on crystals of various thicknesses and orientations. The extremely sharp absorption resonances indicate long dephasing times ( $> 1.5$  ns). Thus resonant single mode excitation might provide an efficient way to create a dense coherent population of dipole forbidden excitons.

The work was supported by the Deutsche Forschungsgemeinschaft and the QuIST program of DARPA.

- [1] K. Cho, Phys. Rev. B **14**, 4463 (1976).
- [2] G. L. Bir and G. E. Pikus, *Symmetry and Strain-Induced Effects in Semiconductors* (John Wiley and Sons, New York, 1974).
- [3] E. L. Ivchenko and G. E. Pikus, *Superlattices and Other Heterostructures* (Springer-Verlag, Berlin, 1995).
- [4] For an overview see M. Bayer *et al.*, Phys. Rev. B **65**, 195315 (2002), and references therein.
- [5] See, e.g., U. Rössler and H. R. Trebin, Phys. Rev. B **23**, 1961 (1981); H. Fu, L.-W. Wang, and A. Zunger, Phys. Rev. B **59**, 5568 (1999).
- [6] V. T. Agekyan, Phys. Status Solidi (a) **43**, 11 (1977).
- [7] G. F. Koster *et al.*, *Properties of the Thirty-Two Point Groups* (MIT Press, Cambridge, MA, 1963).
- [8] R. J. Elliott, Phys. Rev. **124**, 340 (1961).
- [9] D. Fröhlich *et al.*, Phys. Rev. Lett. **67**, 2343 (1991).
- [10] J. S. Schwinger *et al.*, *Classical Electrodynamics* (Perseus Books, Reading, MA, 1998).
- [11] The LR exchange interaction was also recently analyzed by Moskalenko *et al.* [Phys. Status Solidi (b) **213**, 377 (1999)], who, however, treated it as an effective dipole-dipole interaction and did not take the off-diagonal matrix elements into account. As these are of the same magnitude as the diagonal terms, they should not be neglected.
- [12] J. M. Luttinger, Phys. Rev. **102**, 1030 (1956).
- [13] G. Kuwabara, M. Tanaka, and H. Fukutani, Solid State Commun. **21**, 599 (1977).
- [14] Because of the thickness of the crystal the light is fully absorbed within a comparably broad spectral range.
- [15] The use of a much larger set of data than shown here explains the small systematic discrepancies between experiment and theory in Fig. 3(b).